Hindawi
Mathematical Problems in Engineering
Volume 2021, Article ID 9984934, 21 pages
https://doi.org/10.1155/2021/9984934

Research Article

Optimum Design of Straight Circular Channels Incorporating Constant and Variable Roughness Scenarios: Assessment of Machine Learning Models

Majid Niazkar

Department of Civil and Environmental Engineering, Shiraz University, Shiraz, Iran

Correspondence should be addressed to Majid Niazkar; mniazkar@shirazu.ac.ir

Received 4 April 2021; Accepted 12 August 2021; Published 25 August 2021

Academic Editor: Samuel Yousefi

In this study, two machine learning (ML) models named as artificial neural network (ANN) and genetic programming (GP) were applied to design optimum canals with circular shapes. In this application, the earthwork and lining costs were considered as the objective function, while Manning's equation was utilized as the hydraulic constraint. In this design problem, two different scenarios were considered for Manning's coefficient: (1) constant Manning's coefficient and (2) the experimentally proved variation of Manning's coefficient with water depth. The defined design problem was solved for a wide range of different dimensionless variables involved to produce a large enough database. The first part of these data was used to train the ML models, while the second part was utilized to compare the performances of ANN and GP in optimum design of circular channels with those of explicit design relations available in the literature. The comparison obviously indicated that the ML models improved the accuracy of the circular channel design from 55% to 91% based on two performance evaluation criteria. Finally, application of the ML models to optimum design of circular channels demonstrates a considerable improvement over the explicit design equations available in the literature.

1. Introduction

The need for conveying water using manmade lined canals is inevitable. Basically, channel design is the determination of channel properties so that not only can it convey required amount of water properly but also it is designed based on some controlling criteria. The former demands taking into account hydraulic conditions of flow passing through the channel under consideration, while the latter delineates how to define the problem statement. For instance, when the budget of channel construction is the most important key factor, a cost-minimization problem is particularly sought. As a result, the quest for optimum design of channels has brought about an active field of research in hydraulic engineering [1, 2]. These studies can help hydraulic engineers to design channels with different section shapes including (1) linear sections [3], (2) curved sections [4], and (3) linear-curved sections [5, 6]. Since the focus of this study is devoted to optimum design of circular channels, the literature is reviewed considering studies conducted exclusively on design of circular canals.

Among various studies on optimum channel design, design of circular channels, as one of conventional sections, was considered among the earliest attempts. Swamee [7] developed design equations for the best hydraulic circular section by minimizing flow area. Swamee [8] derived section variables of an optimal circular channel for viscous flow. Swamee et al. [8] defined a general construction cost incorporating a lining cost and suggested explicit equations for optimum design of lined circular channels. These equations were derived by minimizing the general construction cost. Swamee et al. [9] presented explicit relations for the optimum design of canals with circular shapes by minimizing earthwork cost of channel construction. In two previous

studies, Swamee's resistance equation was considered as the hydraulic constraint. Swamee and Kashyap [10] solved the differential equation that governs seepage flow using a finite difference scheme for a large number of independent dimensionless variables of a circular section. The outcome of this analysis yielded the proposal of an explicit equation for seepage from circular canals, which was used for developing explicit equations for optimum design of circular channels with minimum seepage loss. These equations were improved to take into account the impact of a drainage layer occurred at a shallow depth [11]. Aksoy and Altan-Sakarya [3] proposed two models for calculating the optimal section variables of circular channels by minimizing earthwork and lining costs, while Manning's equation was the hydraulic constraint. Niazkar and Afzali [12] utilized the Modified Honey Bee Mating Optimization algorithm to minimize the generalized form of the construction cost. They developed new explicit equations for optimum design of lined circular channels and compared the performance of their equations with that of Swamee et al.'s [8] equations and Aksoy and Altan-Sakarya's [3] equations. Their comparison indicated that Niazkar and Afzali's [12] explicit relations outperformed the other ones. Swamee and Chahar [13] recommended explicit equations for the optimum design of circular sections when they should transport a requisite sediment discharge. Since the sediment velocity has a direct relationship with the channel hydraulic radius, the optimum design problem reduced to the maximization of the hydraulic radius. Since no reliable resistance equation is available for computing flow in rigid boundary channels that carry sediment, a sediment discharge relation was selected as the constraint. This relation was obtained by substituting a limit deposit velocity into the head loss formula of sediment transport through pipes in heterogeneous suspension [13]. More recently, Niazkar et al. [1] minimized the earthwork and lining construction costs by taking into account the variation of Manning's coefficient with water depth. They proposed explicit relations for the optimum design of circular channels. According to the conducted literature review, the optimum design of circular channels was basically introduced as an optimization problem, while a hydraulic constraint was imposed based on the design priority. Additionally, most of previous studies recommended equations to design circular channels explicitly.

Despite previous efforts on estimating optimum channel properties with circular shapes, there is still a need to explore further in favor of improving the optimum results. In this regard, this study aims not only to revisit the optimum design problem of open channels with circular cross sections but also to possibly improve estimations of channel properties. In this regard, artificial intelligence (AI) and machine learning (ML) models, which have been proven to be powerful estimation tools for different water resources problems in literatures [14–17], have not been applied for optimum design of canals with circular sections. Since ML models have been successfully used in estimation of the optimum geometric variables of lined channels with triangular, rectangular, and trapezoidal sections [18] and predicting channel geometries with trapezoidal and rectangular sections considering water loss [19], applying AI models to the optimum design of lined circular channels may improve the accuracy of this design.

Since determining the optimum values of channel properties in a water-conveyance project can significantly lower the required budget for excavating and lining, exploring for estimating the optimum values of channel properties is of great importance. In this study, the optimum design of lined canals with circular shapes is tackled by applying two ML methods (artificial neural network (ANN) and genetic programming (GP)) for estimating channel properties in for two scenarios: (1) constant and (2) variable Manning's coefficients. To the best of author's knowledge, it is the first time that ML methods has been exploited to estimate channel properties of lined circular channels. The performances of these ML models were compared with those of the explicit design equations present in the literature. In this regard, the problem statement of the circular channel design is introduced in the next section. In the same section, different models used for estimating circular channel properties are reviewed. Afterwards, the results of applying ML to the channel design with circular shapes are presented and discussed for constant and variable roughness scenarios.

2. Methods and Materials

2.1. Problem Statement of Optimum Channel Design. Channels are one of the most widely used hydraulic structures to convey water through either short or long distances. Generally, the construction cost of canals is counted as one of the main parameters, which plays the key role in real-life water-conveyance projects. The quest for a reality-based definition for channel design problem has been addressed in the literature by various studies. In this regard, one of the approaches for channel design is to treat it as an optimization problem, while the construction cost is assumed as an objective function. Although various factors may play roles in the cost of constructing a channel, considering all of them in a problem statement is not possible mostly because some of them are not predictable [12]. Nevertheless, considering dominant factors is required to address a close-to-reality solution for canal construction projects.

The total construction cost per unit length of a typical lined channel (C) is one the most generalized form of construction costs available in literatures [1, 3, 8, 12]. It assumed three construction components: (1) the earthwork cost per unit volume (β_E), (2) the additional earthwork cost associated with different earthwork costs in different depths (β_A), and (3) the lining cost per unit area (β_L). Therefore, the objective function consists of three costs [8]:

$$C = \beta_L P + \beta_E A + \beta_A \int_0^{y_n} a\,d\eta, \tag{1}$$

where P is the wetted perimeter, A is the channel cross section area, y_n is the water normal depth, a is the flow area at height η, and dη is the unit length of earthwork at height η, where η represents the vertical axis of channel geometry.

In order to preserve a hydraulically valid condition for flow throughout the channel, considering a resistance equation is inevitably required in a channel design problem. In this regard, Manning's equation, which is the most common resistance equation in open channels [20], is utilized as the problem constraint:

$$Q - \frac{1}{n} AR^{2/3} \sqrt{S} = 0, \tag{2}$$

where Q is the discharge, n is Manning's coefficient, R is the hydraulic radius, and S is the channel slope.

Using a length-scale parameter $\lambda = (Qn/\sqrt{S})^{3/8}$, the involved dimensional parameters are converted to new dimensionless parameters shown in Table 1. In this table, y is the water depth, r is the channel radius, and $*$ subscript denotes the dimensionless form of a variable. In the optimum design of channels, S in Manning's equation is substituted by the bottom channel slope. Therefore, water depth resulted from Manning's equation is the normal water depth, while the index associated with the normal depth is omitted from y and r for simplification.

Generally, Manning's coefficient may be flow-dependent or flow-independent in open-channel hydraulics [20, 21]. As a result, λ can either be constant or vary with flow. Although

Table 1: Dimensionless parameters involved in the design problem statement.

$C_* = C/\beta_E\lambda^2$	$\beta_{A*} = \beta_A\lambda/\beta_E$	$\beta_{L*} = \beta_L/\beta_E\lambda$	$A_* = A/\lambda^2$
$P_* = P/\lambda$	$y_* = y/\lambda$	$r_* = r/\lambda$	

the former assumption may seem to be more streamlining for practical purposes, the latter one is based on experiments conducted in partially filled circular channels. Based on these experiments [22–25], Manning's coefficient varies with water depth angle (θ) [1]:

$$\frac{n}{n_f} = 1 + 0.18(2\pi - \theta)\left[0.1 + \exp(-0.3\theta)\sin^2(0.38\theta)\right], \tag{3}$$

where n and n_f are Manning's coefficients associated with a partially and completely full cross section, respectively.

Using the dimensionless parameters shown in Table 1, the objective function and the constraint of the design problem of lined circular channels considering variable Manning's coefficients are shown in equation (4) and equation (5), respectively [1]:

$$\text{minimize } C_* = \beta_{L*}\theta r_* + 0.5 r_*(\theta - \sin\theta) + 0.5\beta_{A*} r_* \left[(y_* - r_*)\theta + \frac{4r_*^2 + 2(y_* - r_*)^2}{3r_*^2}\sqrt{r_*^2 - (y_* - r_*)^2}\right], \tag{4}$$

$$\text{subjected to } n_f \times \left\{1 + 0.18(2\pi - \theta)\left[0.1 + \exp(-0.3\theta)\sin^2(0.38\theta)\right]\right\} - \left[0.5 r_*(\theta - \sin\theta)\right]^{5/3}(\theta r_*)^{-2/3} = 0. \tag{5}$$

For better clarification, Figure 1 presents a schematic view of geometric variables involved in the design problem of partially filled circular channels. Particularly, Figure 1 introduces θ for two scenarios: (a) $y > r$ and (b) $y < r$. Based on Figure 1, $\theta/2$ is less than 90 degree for the former and more than 90 degree for the latter, respectively.

When n is assumed to be flow-independent, the objective function of the problem statement is still equation (4) because n does not appear in the cost of channel construction. However, the constraint, which plays the role of a hydraulically feasible condition for flow moving in channels, inevitably depends on Manning's coefficient. Consequently, the constraint for flow-independent n is presented in the following equation [3]:

$$\left\{r_*\left[\pi - 2\sin^{-1}\left(1 - \frac{y_*}{r_*}\right)\right]\right\}^{2/3} - \left\{0.5 r_*^2\left[\pi - 2\sin^{-1}\left(1 - \frac{y_*}{r_*}\right) - 2\left(1 - \frac{y_*}{r_*}\right)\frac{\sqrt{r_*^2 - (r_* - y_*)^2}}{r_*}\right]\right\}^{5/3} = 0. \tag{6}$$

The design problem of lined circular channels for both constant and variable n has been solved in the literature, and various explicit formulas have been suggested for computing the optimum circular channel geometries. These relations are summarized in Table 2. In this table, L in Swamee et al.'s [8] model is equal to $\lambda_1((\varepsilon/\lambda_1) + (8\upsilon\lambda_1/Q))^{0.04}$, where $\lambda_1 = (Q/\sqrt{gS})^{0.4} = \lambda^{32/30}/n^{0.4}g^{0.2}$, g is the gravitational acceleration, ε is the average roughness height of canal surface, and υ is the kinematic viscosity. Among the equations reviewed in Table 2, equations (ix)–(xii) consider variable n, while the rest assume constant n with respect to flow.

2.2. Optimization Algorithm. In this study, the described design problem was solved for two scenarios (constant and variable n) by a well-known optimization algorithm, named Modified Honey Bee Mating Optimization (MHBMO) algorithm. This optimization algorithm has been successfully applied to this specific problem [1, 12]. The MHBMO algorithm

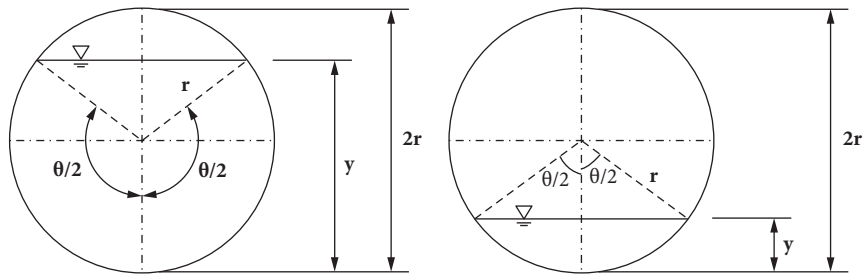

Figure 1: Schematic view of geometric variables of a partially filled circular channel: (a) $y > r$ and (b) $y < r$.

Table 2: Chronological review of explicit equations available for computing circular channel geometries.

Researchers	Equation number	Proposed relation
(a) For flow-independent Manning's coefficient		
Swamee et al. [8]	(i)	$2r = 0.78065L + (0.19375\beta_A L^3/(\beta_E\ L + 13.6232\beta_L))$
	(ii)	$y = 0.39032L(1 + (0.12631\beta_A L^2/(\beta_E L + 12.9379\beta_L)))^{-1}$
Aksoy and Altan-Sakarya [3]-first model	(iii)	$r_* = 1.004 + (0.113\beta_{A*}/\beta_{L*})$
	(iv)	$y_* = 1.004(1 + (0.055\beta_{A*}/\beta_{L*}))^{-1}$
Aksoy and Altan-Sakarya [3]-second model	(v)	$r_* = 1.004 + (0.58\beta_{A*}/(1 + 5.008\beta_{L*}))$
	(vi)	$y_* = 1.004(1 + (0.277\beta_{A*}/1 + 4.937\beta_{L*}))^{-1}$
Niazkar and Afzali [12]	(vii)	$r_* = 1.004 + 0.2358\beta_{A*}^{0.9978}\beta_{L*}^{-0.7749}$
	(viii)	$y_* = 1.004(1.0091 + 3.3182\beta_{A*}^{1.3175}\beta_{L*}^{-1.0878})^{-0.0708}$
(b) For flow-dependent Manning's coefficient		
Niazkar et al. [26]-first model	(ix)	$r_* = 0.9493\beta_{L*}^{0.0202} + 0.3542\beta_{A*}^{1.0351}\beta_{L*}^{-0.702}$
	(x)	$y_* = 1.1663\beta_{L*}^{-0.01} - 0.1557\beta_{A*}^{0.9322}\beta_{L*}^{-0.5489}$
Niazkar et al. [26]-second model	(xi)	$r_* = 0.9539\beta_{L*}^{0.0175} + 0.3501\beta_{A*}^{1.0352}\beta_{L*}^{-0.705}$
	(xii)	$y_* = 1.1598\beta_{L*}^{-0.0114} - 0.1618\beta_{A*}^{1.0695}\beta_{L*}^{-0.5676}$

can be classified as a zero-order optimization algorithm, which was originally inspired from the mating process of honey bees. It has five main controlling parameters, which include the size of the initial population, the number of workers, the queen's speed at the start and end of the mating flight, and the speed reduction factor. The MHBMO controlling parameters were set as recommended in previous studies [12]. Finally, the MHBMO algorithm was merely utilized in this study to compute the optimum values of channel properties with circular shapes, while two ML methods were applied to the optimum properties computed for the circular channels.

2.3. Machine Learning Models. In this study, two ML models are used for estimating the optimum properties of lined circular channels: (1) ANN and (2) GP. Although the applications of ANN and GP have been presented well in the literature of hydraulic engineering [15, 18], this is the first time that these AI models have been utilized for the optimum design of lined circular channels. The feature characteristics of ANN such as training capability, parallel operation, and distributed memory result in their fault resiliency and prediction accuracy. In essence, it compromises a random mapping between two vectors of input and output values. The architecture of ANNs, as shown in Figure 2(a), commonly consists of three layers of neurons, which are invariantly called input, hidden, and output layers, while each layer includes several neurons, and the layers are interrelated by sets of correlation weights. This structure, which provides a high degree of freedom, may yield a robust prediction capability. In this study, a three-layer network with feed-forward back-propagation characteristic was used to train ANN, while the controlling parameters of ANN were selected as the same as the ones used in literature [18].

The second ML model used in this study, i.e., GP, is basically a suitable extension to the genetic algorithm. In essence, it adopts principles of crossover Figure 2(c), mutation Figure 2(d), and survival of the fittest individuals not only to find an optimum solution but also to predict an output vector based on a known input vector. The tree-like structure of GP, as shown in Figure 2(b), consists of functions and terminals, while branches of each tree are connected to a root point. The function set can contain arithmetic operations, Boolean logical operators, and logical or deductive conditions or mathematical functions or any other functions. Furthermore, the terminal set is usually composed of variables, numerical constants, and so on. This characteristic inherently makes GP a powerful estimation tool. The main advantage of GP over regression-based equations is that it can seek for both structures and parameters of the relationship under investigation without the need to assume a shape limit in advance [15]. For applying GP, Discipulus [27] software was used to predict the optimal circular channels, while it has been employed for various

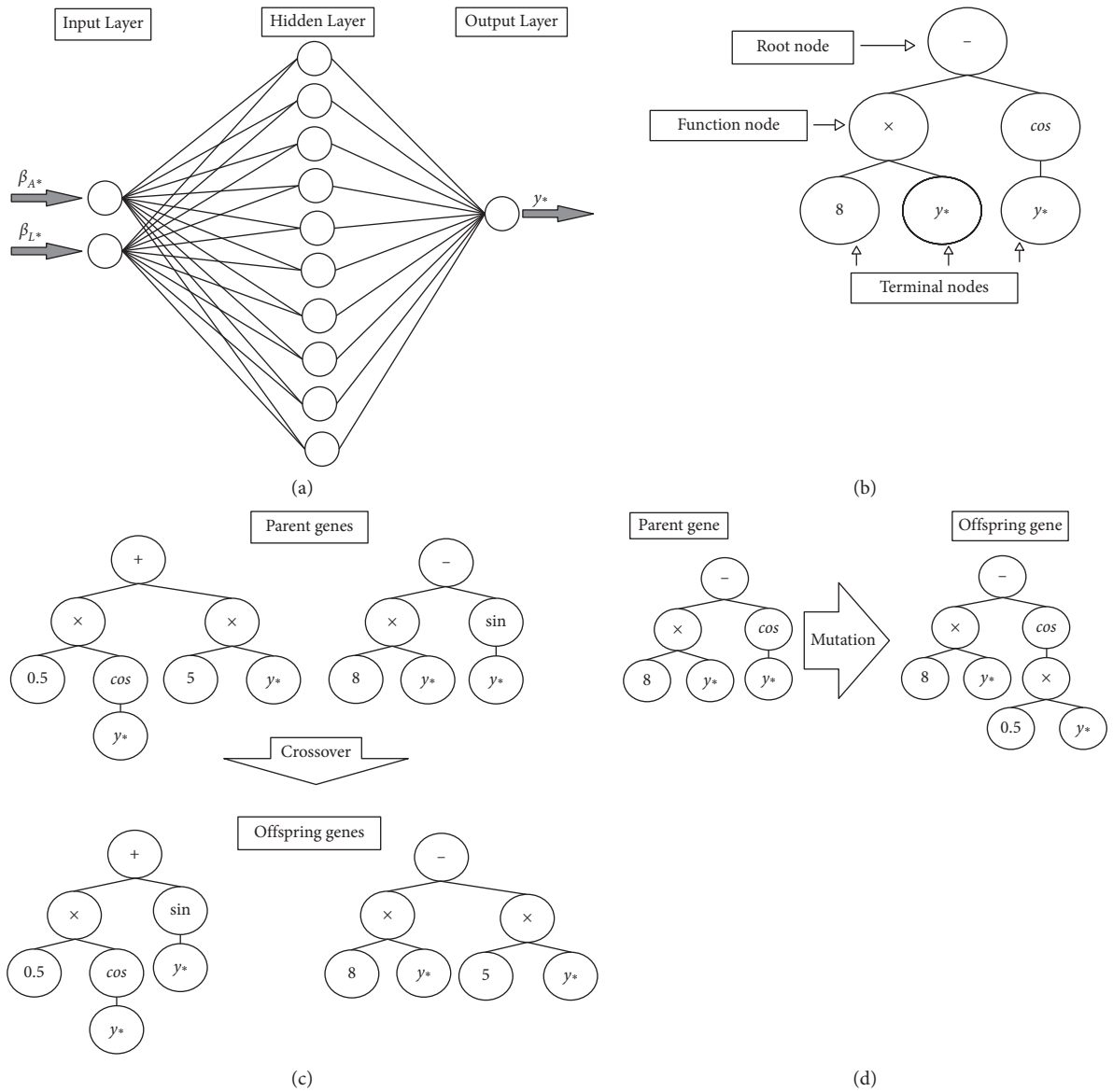

Figure 2: Schematic view of ML models: (a) ANN structure; (b) GP structure; (c) crossover process in GP; (d) mutation process in GP.

applications in water-related fields of study [1]. Finally, the default values of GP parameters presumed in Discipulus software were considered.

2.4. Application of ML Method to Solve the Design Problem. The described design problem of lined circular channels was treated as optimization problem, which was solved by the MHBMO algorithm for two constant and variable roughness scenarios. Each scenario is solved for 210 pairs of β_{A*} and β_{L*}, while the ratio of β_{A*}/β_{L*} is within (0, 2) for all pairs of data, similar to previous studies [3, 12]. By solving this design problem, the optimum channel properties (r_* and y_*) were obtained for various values of β_{A*} and β_{L*}. The optimum values of channel properties and dimensionless cost factors build up a dataset, which was utilized for estimating optimum values of channel properties using different models including ML methods (ANN and GP). The developed data were normalized within the range of (0.0, 1.0) before being used by the ML models. These 210 data for each scenario are depicted in Figure 3. As shown, variations of channel roughness have an inevitable impact on optimum values of r_* and y_*. The data illustrated in Figure 3 are randomly divided into two parts: (1) train data (150 data for each scenario) and (2) test data (60 data for each scenario). The former was utilized for training the ML models, while the latter was employed for testing stage. The detailed description of the data division is presented in literature [26].

2.5. Performance Evaluation Criteria. In order to compare performances of explicit equations with those of the ML models for calculating the optimum water depth and channel radius of circular channels, five performance evaluation criteria are used in this study [26]. These criteria

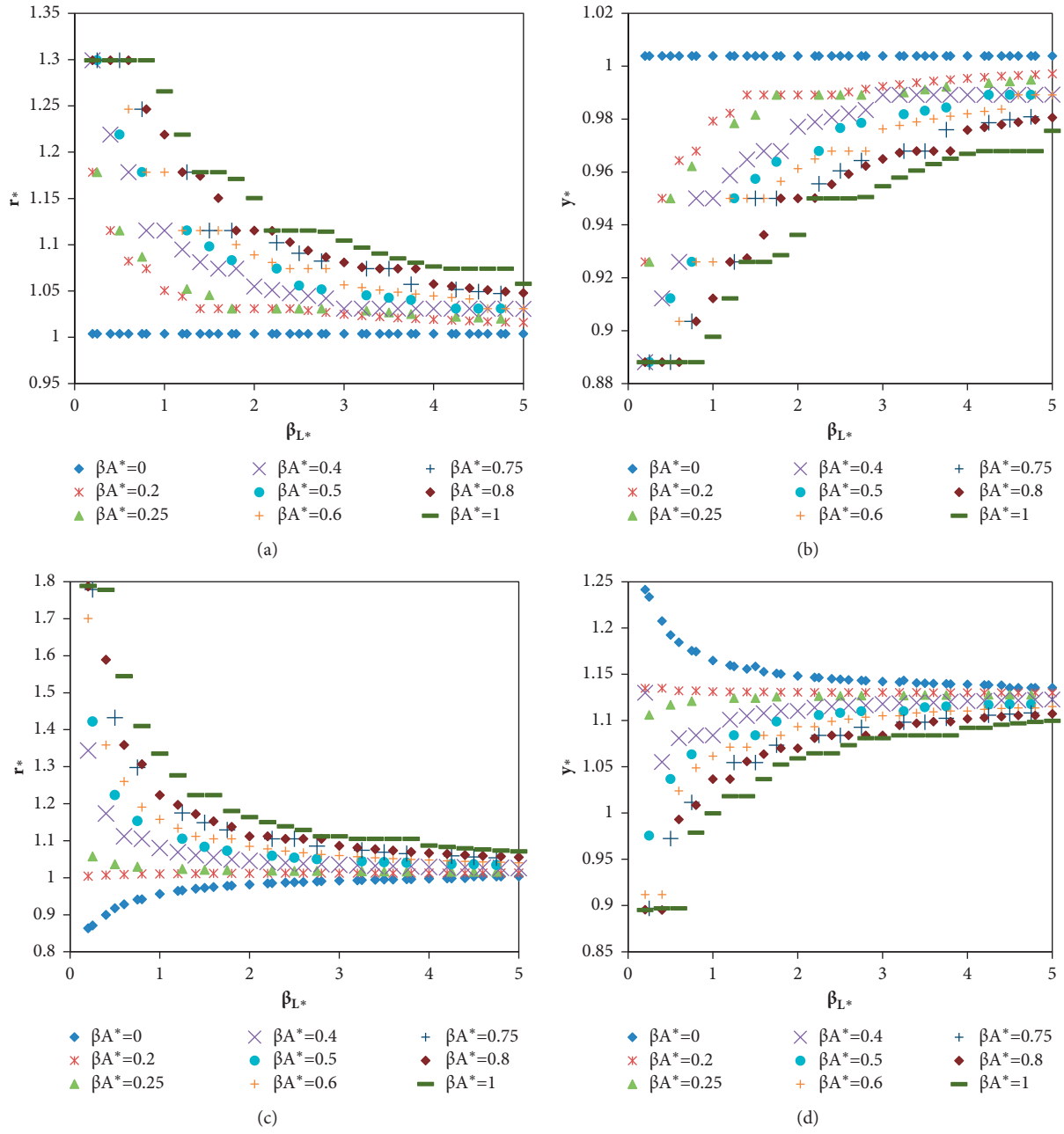

FIGURE 3: Variations of r_* and y_* for different β_{A*} and β_{L*}: (a) constant roughness; (b) constant roughness; (c) variable roughness; (d) variable roughness.

include (1) root mean square error (RMSE), (2) mean absolute error (MAE), (3) mean absolute relative error (MARE), (4) relative error (RE), and (5) coefficient of determination (R^2). Among these criteria, RE can be computed for each set of y_* and r_*, whereas other four criteria are reported for either train or test data. The five indices are written in terms of y_* in the following equations, respectively, while they can be written for r_*, too [26]:

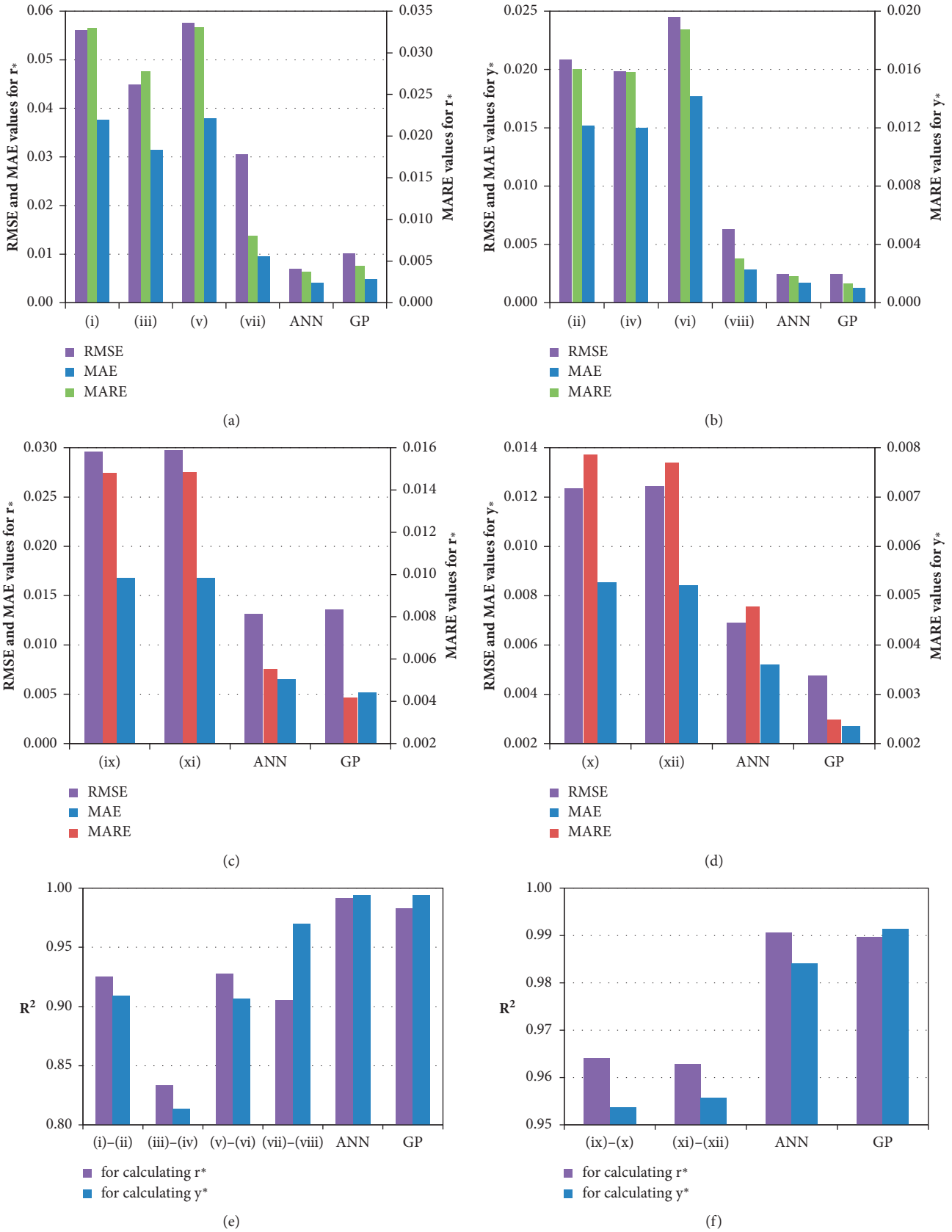

FIGURE 4: Comparison of different models for calculating the optimum r_* and y_*: (a) constant roughness; (b) constant roughness; (c) variable roughness; (d) variable roughness; (e) constant roughness; (f) variable roughness.

$$\begin{aligned}
\mathrm{RMSE} &= \sqrt{\frac{1}{N}\sum_{i=1}^{N}\left(y_{*,\mathrm{database}} - y_{*,\mathrm{estimated}}\right)^2},\\
\mathrm{MAE} &= \frac{1}{N}\sum_{i=1}^{N}\left|y_{*,\mathrm{database}} - y_{*,\mathrm{estimated}}\right|,\\
\mathrm{MARE} &= \frac{1}{N}\sum_{i=1}^{N}\left|\frac{y_{*,\mathrm{database}} - y_{*,\mathrm{estimated}}}{y_{*,\mathrm{database}}}\right| \times 100,\\
\mathrm{RE} &= \frac{y_{*,\mathrm{estimated}} - y_{*,\mathrm{database}}}{y_{*,\mathrm{database}}},\\
R^2 &= \left(\frac{\sum_{i=1}^{N}\left[\left(y_{*,\mathrm{database}} - \left(\sum_{i=1}^{N} y_{*,\mathrm{database}}/N\right)\right)\left(y_{*,\mathrm{estimated}} - \left(\sum_{i=1}^{N} y_{*,\mathrm{estimated}}/N\right)\right)\right]}{\sqrt{\sum_{i=1}^{N}\left[\left(y_{*,\mathrm{database}} - \left(\sum_{i=1}^{N} y_{*,\mathrm{database}}/N\right)\right)^2\left(y_{*,\mathrm{estimated}} - \left(\sum_{i=1}^{N} y_{*,\mathrm{estimated}}/N\right)\right)^2\right]}}\right)^2,
\end{aligned} \tag{7}$$

where $y_{*,\mathrm{database}}$ and $y_{*,\mathrm{estimated}}$ are the database and estimated dimensionless water depth, respectively.

3. Results and Discussion

The results obtained by applying ML methods to the design problems are plotted in Appendix A. Furthermore, the output equations achieved by ANN for each roughness scenario (constant or variable n) and each channel property (r_* or y_*) are presented in Appendix B. Finally, the results of different methods are compared separately for each roughness scenario in the following.

3.1. Results of the Constant Roughness Scenario. As shown in Table 2, four models are available in the literature for computing circular channel geometries when n is assumed constant in respect with flow. The performances of these explicit equations are compared with those of the ML models for computing r_* and y_* in Figures 4(a) and 4(b) for the test data, respectively. According to Figure 4, ML models suggested in this study perform much better than all explicit equations based on all four criteria for flow-independent n. Among explicit equations for calculating optimum r_* for constant n, equation (vii) (Table 2) achieved the best RMSE, MAE, and MARE, while equation (v) (Table 2) yielded the best R2, as shown in Figure 4(e). Also, Figure 4 shows that equation (viii) (Table 2) reaches the best values for the four criteria considered for calculating optimum y_* for constant n. Additionally, Figure 4 demonstrates that ANN calculates closer r_* to the optimum solutions for constant n, while ANN and GP have quite the same performances for calculating optimum y_* for constant n. Based on RMSE values shown in Figure 4, the improvement made for predicting r_* and y_* varies between 61% and 88%, while the ML models improved the MARE values of r_* and y_* estimated by the available explicit equations between 54% and 91%. Consequently, Figure 4 obviously indicates that the ML models result in much closer values of r_* and y_* to the optimum solutions for design of lined circular channels in comparison with other models available in the literature for constant roughness.

Figures 5(a) and 5(b) depict relative errors of r_* and y_* predicted by the ML models for the test data by assuming flow-independent n. As shown, RE values computed by ANN for predicting r_* and y_* are placed within [−0.0179, 0.0293] and [−0.0106, 0.0040], respectively. Moreover, the corresponding bounds of RE values for calculating r_* and y_* by GP are [−0.0455, 0.0198] and [−0.0151, 0.0067], respectively. Comparing these four ranges of RE values shows that the AI models achieved a lower bound of RE values for calculating r_* when n is assumed to be invariant of flow. Furthermore, the average of absolute RE achieved by ANN is 0.037 and 0.0018 for computing r_* and y_*, while the corresponding values obtained by GP are 0.0044 and 0.0013, respectively. These values also indicate that the ML models reached a lower average of absolute RE when they calculated y_* rather than r_*. Among these two ML models, GP yielded a lower average of absolute RE for predicting y_*, while ANN resulted a lower average of absolute RE for calculating r_*.

The confidence limits of r_* and y_* estimated by different models are compared with the benchmark solutions for constant roughness in Figures 6(a) and 6(b), respectively. According to Figure 6(a) (equation (vii) in (Table 2)), ANN and GP achieved much closer confidence limits to that of the benchmark solutions in comparison to other models. Furthermore, Figure 6(b) depicts that equation (viii) (Table 2) and GP obtained close confidence limits to the benchmark confidence limit of y_*. However, Figure 6(b) shows that ANN failed to predict y_* close to the benchmark solutions under the constant roughness scenario. Thus, investigating the confidence limits of r_* and y_* for constant roughness reveals that GP performed very well, whereas ANN merely provided accurate estimations for r_*.

Bland–Altman plots for r_* and y_* estimated by ANN and GP are presented in Figures 7 and 8, respectively. As

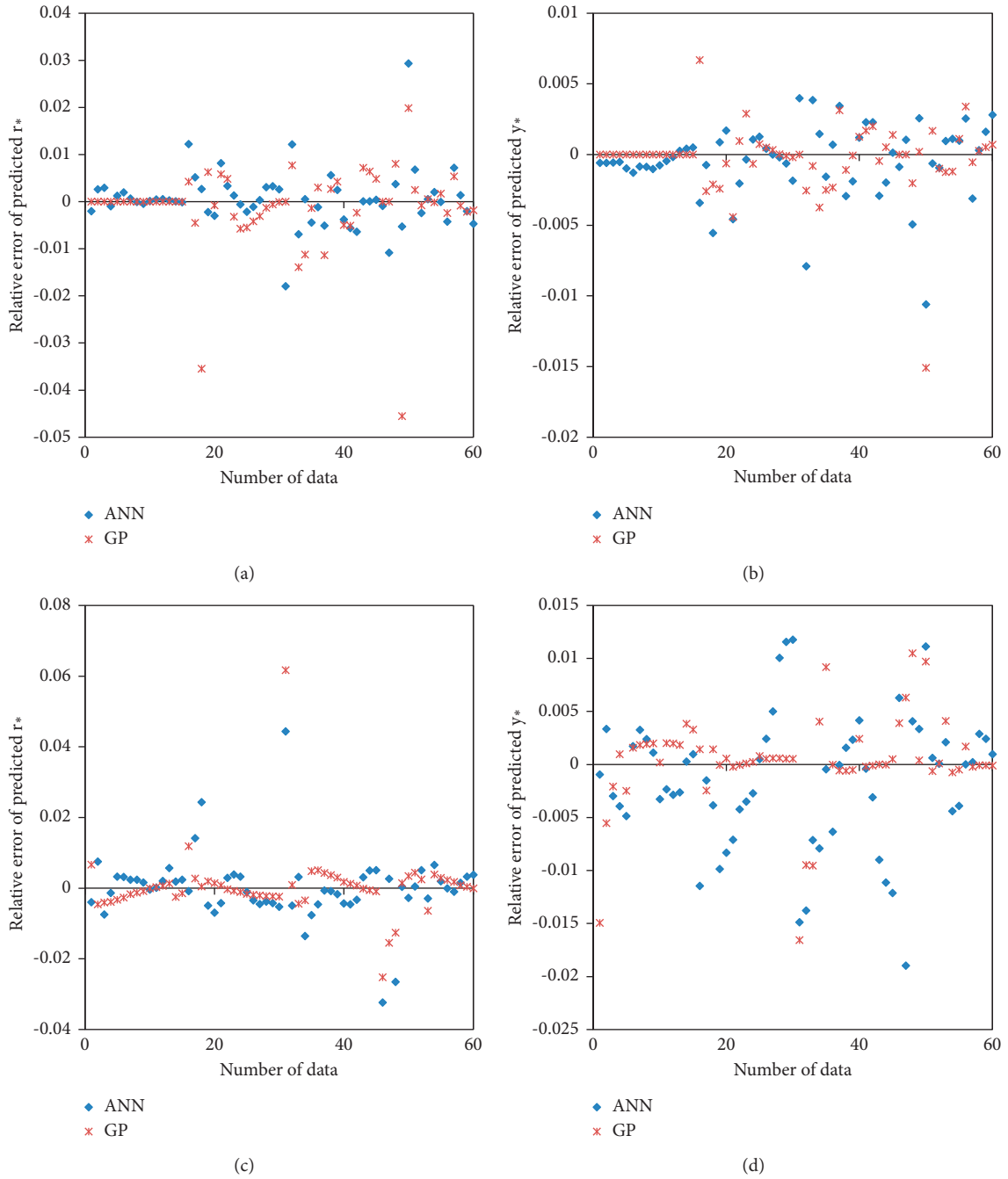

FIGURE 5: Relative error for the optimum r_* and y_* predicted by ANN and GP for the test data: (a) constant roughness; (b) constant roughness; (c) variable roughness; (d) variable roughness.

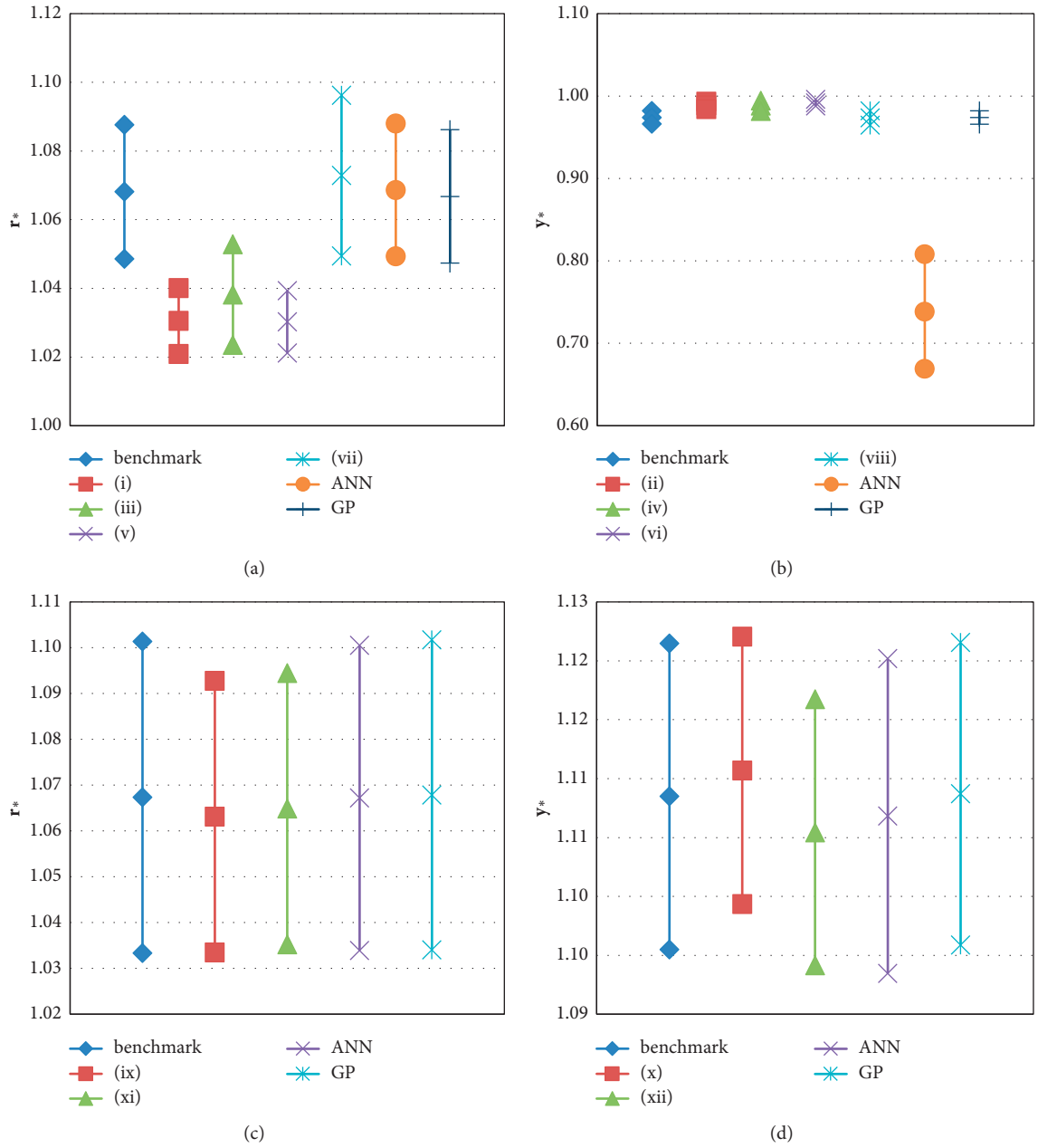

FIGURE 6: Confidence limits for the optimum r_* and y_* predicted by different models for the test data: (a) constant roughness; (b) constant roughness; (c) variable roughness; (d) variable roughness.

shown, the horizontal axis of a Bland–Altman plot is average of measured and estimated values for each data point, while the difference of measured and estimated values is illustrated on the vertical axis. In addition, the mean difference of all data points is a horizontal solid line, while two dashed lines denote ±1.96 standard deviation from the mean difference. In this regard, when 95% of data points of the Bland–Altman plot are placed between the two mentioned dashed lines, the estimated values are in agreement with the benchmark solutions. In other words, this scatter plot can help determine whether r_* and y_* predicted by the ML methods are consistent with the benchmark solutions. According to Figure 7(a), the r_* values estimated by ANN are in agreement with the benchmark solutions as most of points on the corresponding Bland–Altman plot fall between dashed lines associated with ±1.96 standard deviation from the mean difference. However, Figure 7(b) shows that there is a difference between the ANN estimations of y_* and the benchmark solutions for the constant roughness scenario. Furthermore, Figures 8(a) and 8(b) imply that r_* and y_* predicted by GP are in good agreement with the benchmark solutions, respectively. Therefore, GP performed acceptably consistent with benchmark solutions for predicting channel properties under the constant roughness scenario, while ANN only estimated consistent r_* values in comparison with the benchmark solutions.

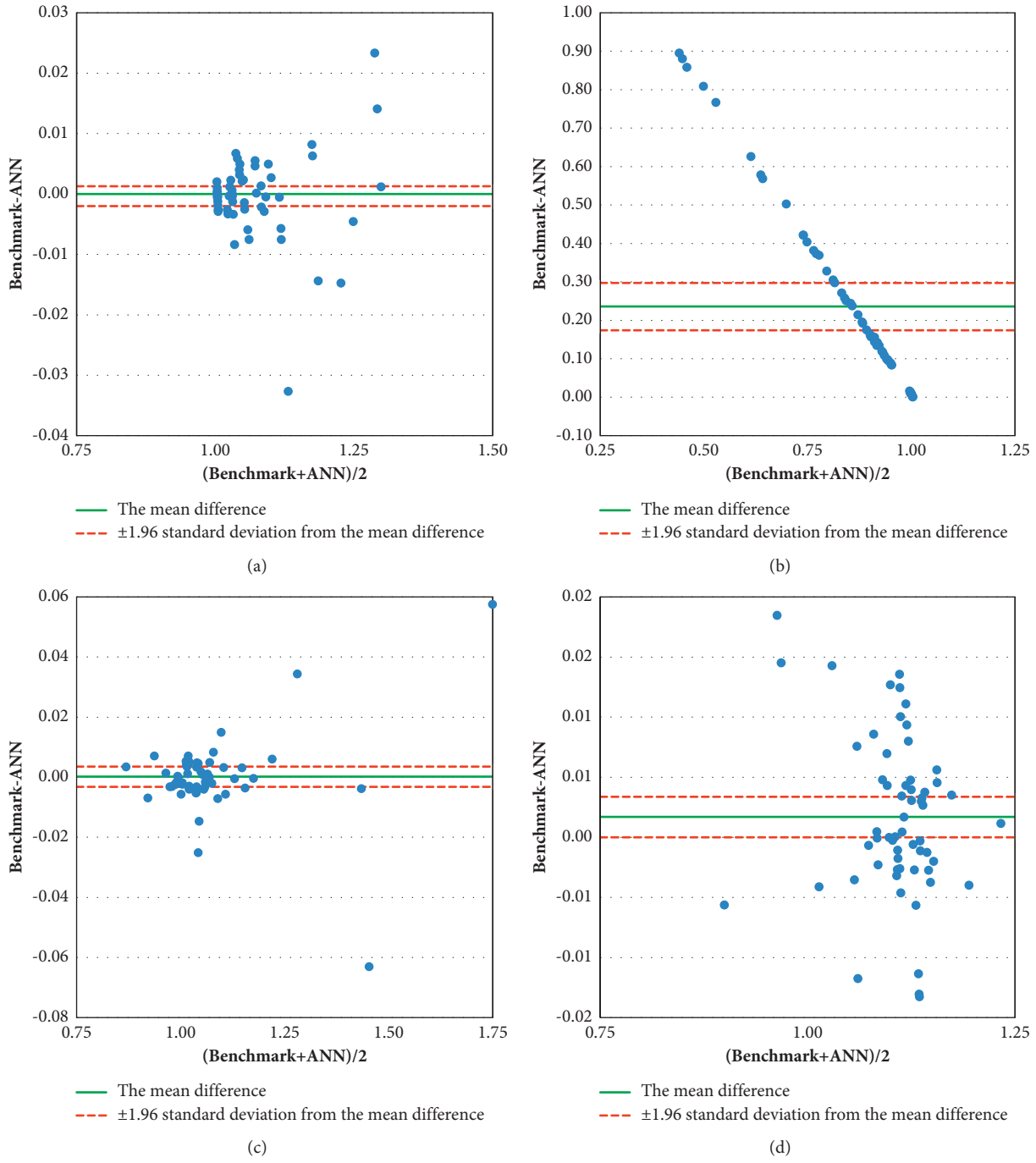

Figure 7: Bland–Altman plots for the optimum r_* and y_* predicted by ANN for the test data: (a) r_* for constant roughness; (b) y_* for constant roughness; (c) r_* for variable roughness; (d) y_* for variable roughness.

3.2. Results of the Variable Roughness Scenario. Two models presented in Table 2 have been proposed to design circular lined canals for flow-dependent n. Figure 4(c) compares the performances of the ML models with those of equations (ix) and (xi) (Table 2) for computing r_* for the test data. As shown, the ML models outperformed the explicit equations available in the literature for predicting optimum r_* values based on all four criteria considered. Additionally, ANN and GP have quite similar performances in calculating r_* for the variable roughness scenario. The performances of the ML models are compared with those of explicit equations in Figure 4(d) for estimating y_* for the test data. The results indicate that both ML models achieved much closer values to the optimum solutions, while GP obtained slightly better results than ANN for calculating optimum y_* for variable n. According to Figure 4, the ML models suggested in this study improved the calculation of r_* up to 55% and 62% based on RMSE and MARE, respectively, while more than 61% and 68% improvements were made to

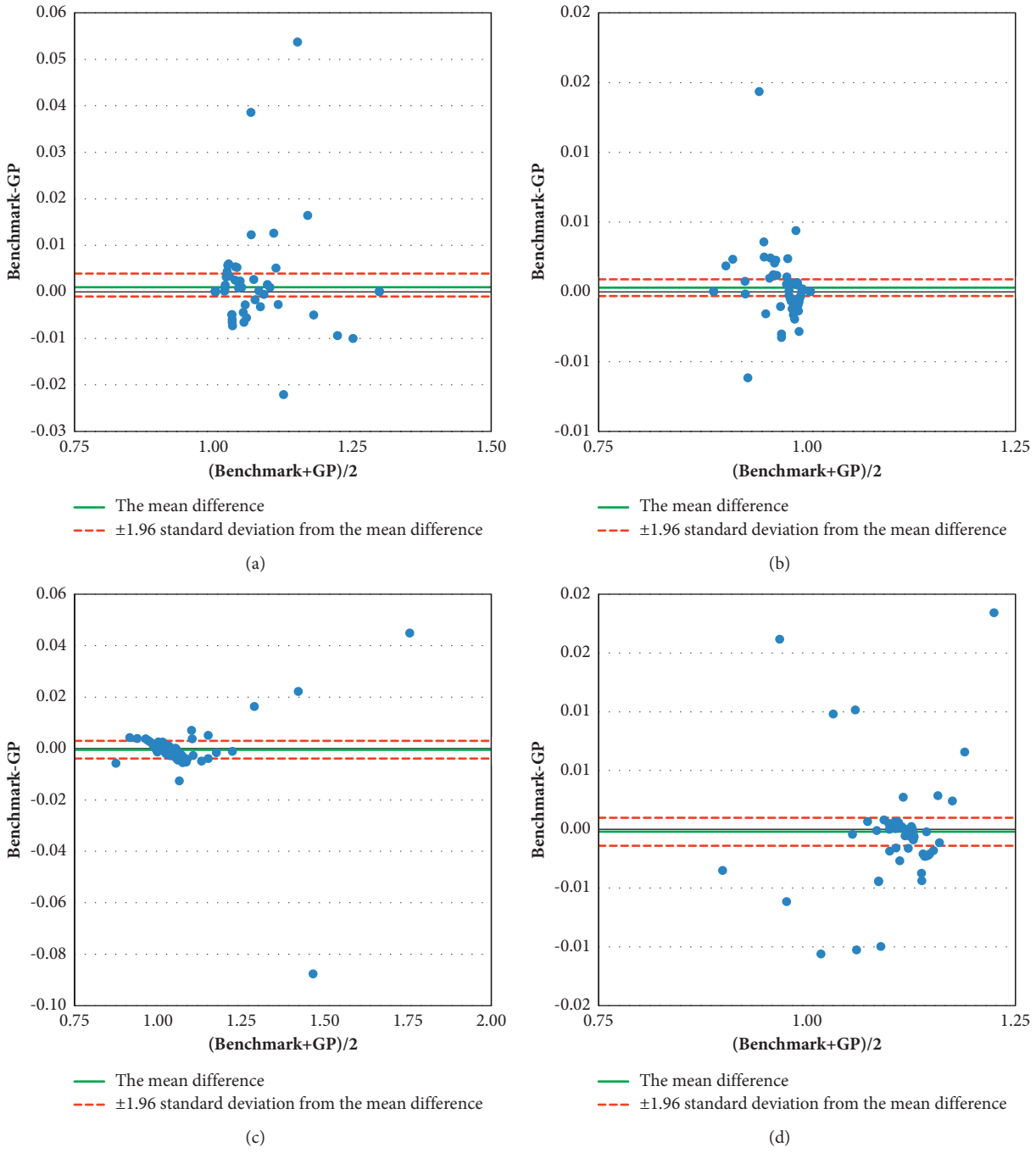

Figure 8: Bland–Altman plots for the optimum r_* and y_* predicted by GP for the test data: (a) r_* for constant roughness; (b) y_* for constant roughness; (c) r_* for variable roughness; (d) y_* for variable roughness.

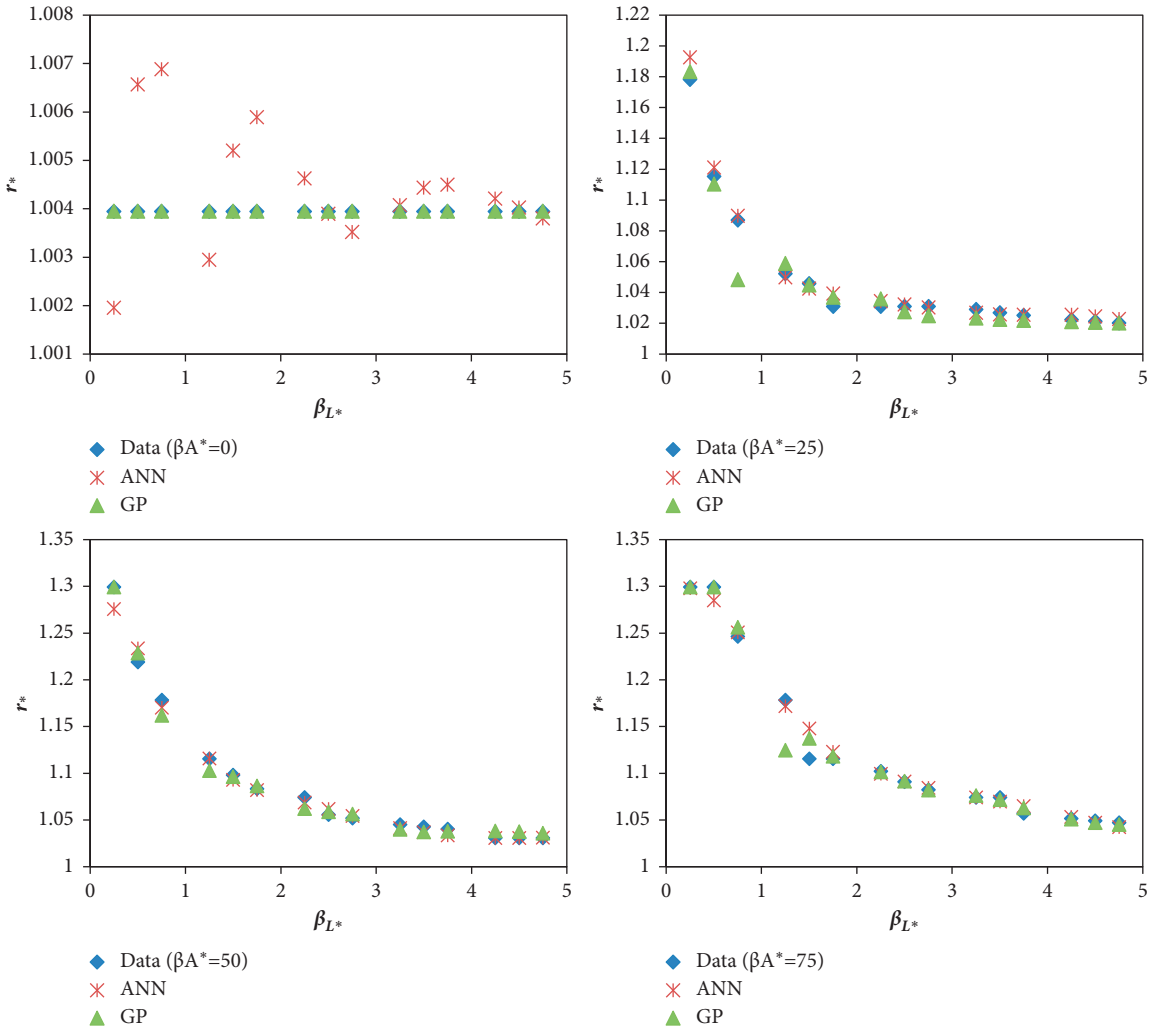

FIGURE 9: Comparison of the benchmark values of r^* with the estimations made by ANN and GP for the constant n scenario for the test data.

RMSE and MARE by the ML models in estimating y_* in comparison with the explicit equations. Therefore, Figure 4 clearly demonstrates that the ML models reached much closer results to the optimum solutions in design of a lined circular channel for flow-dependent n.

For flow-independent n, the relative errors of r_* and y_* calculated by the ML models are presented in Figures 5(c) and 5(d), respectively. As shown, the horizontal axis denotes the number of the test data, while the vertical axis is RE. According to Figure 5(c), the ranges of RE for r_* predicted by ANN and GP are [−0.0324, 0.0444] and [−0.0252, 0.0617], respectively. These bounds demonstrate that the minimum RE of r_* was achieved by ANN, while the maximum RE of r_* was obtained by GP. Moreover, the average values of absolute RE of r_* estimated by ANN and GP are 0.0055 and 0.0042, respectively. These results indicate that ANN performed slightly better than GP for computing r_* in terms of the average of absolute RE for variable roughness scenario. Based on Figure 5(d), RE values calculated by ANN and GP for predicting y_* vary within [−0.0190, 0.0118] and [−0.0166, 0.0105], respectively. Thus, both maximum and minimum RE values were achieved by ANN, which implies that GP has a lower bound of RE values. Furthermore, the average values of absolute RE obtained by ANN and GP for predicting y_* are 0.0048 and 0.0025, respectively. This also indicates that GP performs marginally better than ANN based on the average of absolute RE. In summary, GP yielded a lower average of absolute RE values for predicting y_*, while ANN reached a lower average of absolute RE values for calculating r_*. Regarding each scenario and metrics considered, GP and ANN had slightly different performances, while they both outperformed the explicit equations

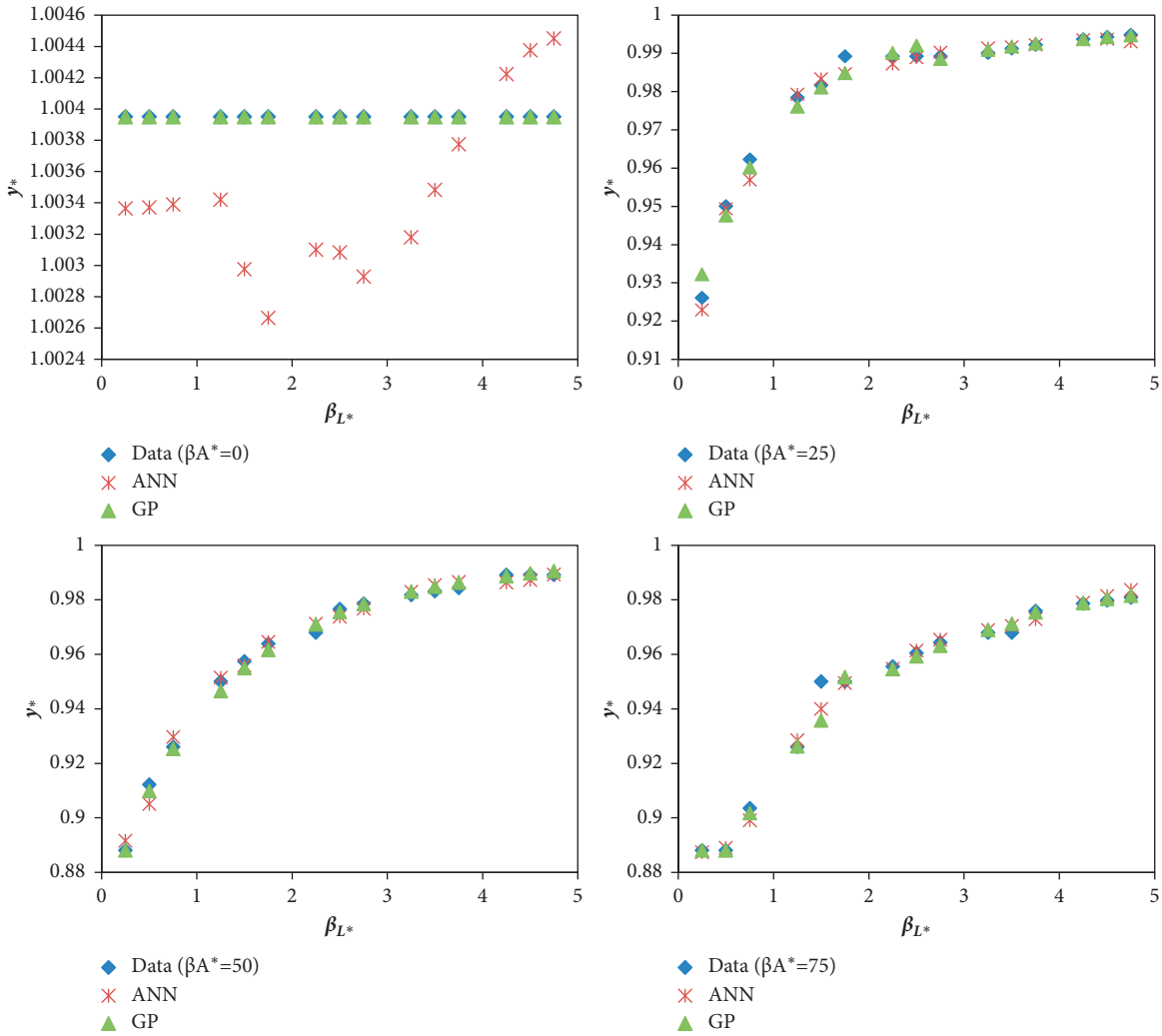

FIGURE 10: Comparison of the benchmark values of y^* with the estimations made by ANN and GP for the constant n scenario for the test data.

available in the literature for predicting r_* and y_* for both constant and variable roughness scenarios.

Figures 6(c) and 6(d) depict the confidence limits of different models under the variable roughness scenario. As shown, both ANN and GP estimated r_* and y_* within the benchmark solutions. Therefore, the ML methods predicted channel properties with high accuracy when a variable n is assumed. Moreover, Figure 6(c) indicates that equations (ix) and (xi) (Table 2) underestimated the maximum r_* in comparison with the benchmark solutions, whereas the ML methods performed adequately for estimating both minimum and maximum r_*. Additionally, Figure 6(d) shows that the maximum and minimum y_* of the benchmark solutions were not estimated acceptably by equations (x) and (xii) (Table 2), respectively, whereas the ML methods, GP in particular, predicted the maximum and minimum y_* close to those of benchmark solutions. Thus, the comparison of confidence limits of channel properties under the variable roughness scenario demonstrates high performance of the ML methods over the existing methods in the literature.

Investigating the Bland–Altman plots for the optimum r_* under the variable roughness scenario Figures 7(c) and 8(c) reveals that the ML estimations are placed with the 95% confidence limit of the corresponding plots. Consequently, GP and ANN provided r_* estimations consistent with the benchmark solution. Likewise, Figure 8(d) obviously indicates the agreement between the y_* values estimated by GP and the benchmarks solutions under the variable roughness scenario. On the contrary, Figure 7(d) shows that most of ANN estimations for y_* fall out of the accepted range, which indicates a difference between ANN predictions and the benchmark solutions. In summary, Figures 7 and 8 demonstrate that GP predicted channel properties are consistent with the benchmark solutions under constant and variable roughness scenarios. These figures also indicate that only the r_* values predicted by ANN are in agreement with the

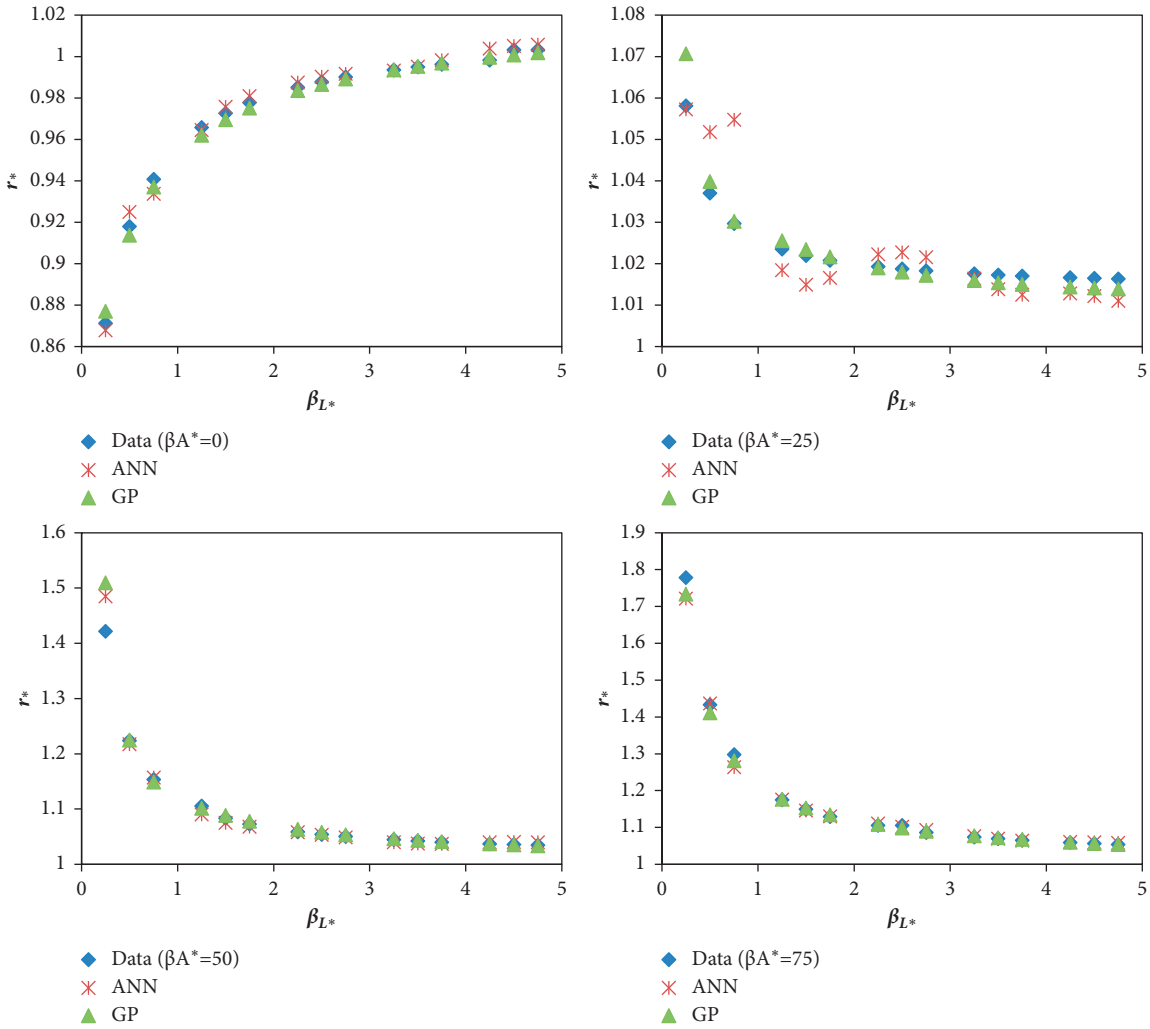

FIGURE 11: Comparison of the benchmark values of r^* with the estimations made by ANN and GP for the variable n scenario for the test data.

benchmark solutions. In conclusion, the accuracy achieved by applying the ML models over the explicit equations implies that these models can be considered as a suitable alternative for design of open channels with circular sections.

3.3. Advantages, Limitations, and Recommendation for Future Works. Since variables involved in the design problem were normalized, the solutions can embrace a variety combination of values of variables with dimensions, which shows the generality of the solutions presented in this study. According to the results of the comparative analysis, the ML methods perform better than equations available in the literature for estimating the optimum values of circular channel properties. This is an advantage of ML methods over the existing models for the same purpose. Furthermore, the ML methods (ANN and GP) have more flexibility to capture the variations of r_* and y_* for different β_{A*} and β_{L*} values in comparison to available formulas. This makes the ML methods more suitable for predicting optimum values of r_* and y_*. Additionally, estimating using the ML methods considered in this study require running the learned machine for any set of β_{A*} and β_{L*} values. This characteristic indicates that the ML methods performed as a black box method and did not present an ML-based simple equation. This feature is likely to be interpreted as a disadvantage for an engineer who prefers to work with mathematical equations when it comes to design optimum circular channels. In a bid to overcome this shortcoming, it is suggested to employ improved version of the ML methods, e.g., Multi-Gene GP, which provide mathematical equations. Finally, the uncertainty in β_{A*} and β_{L*} values is suggested to be investigated in future studies.

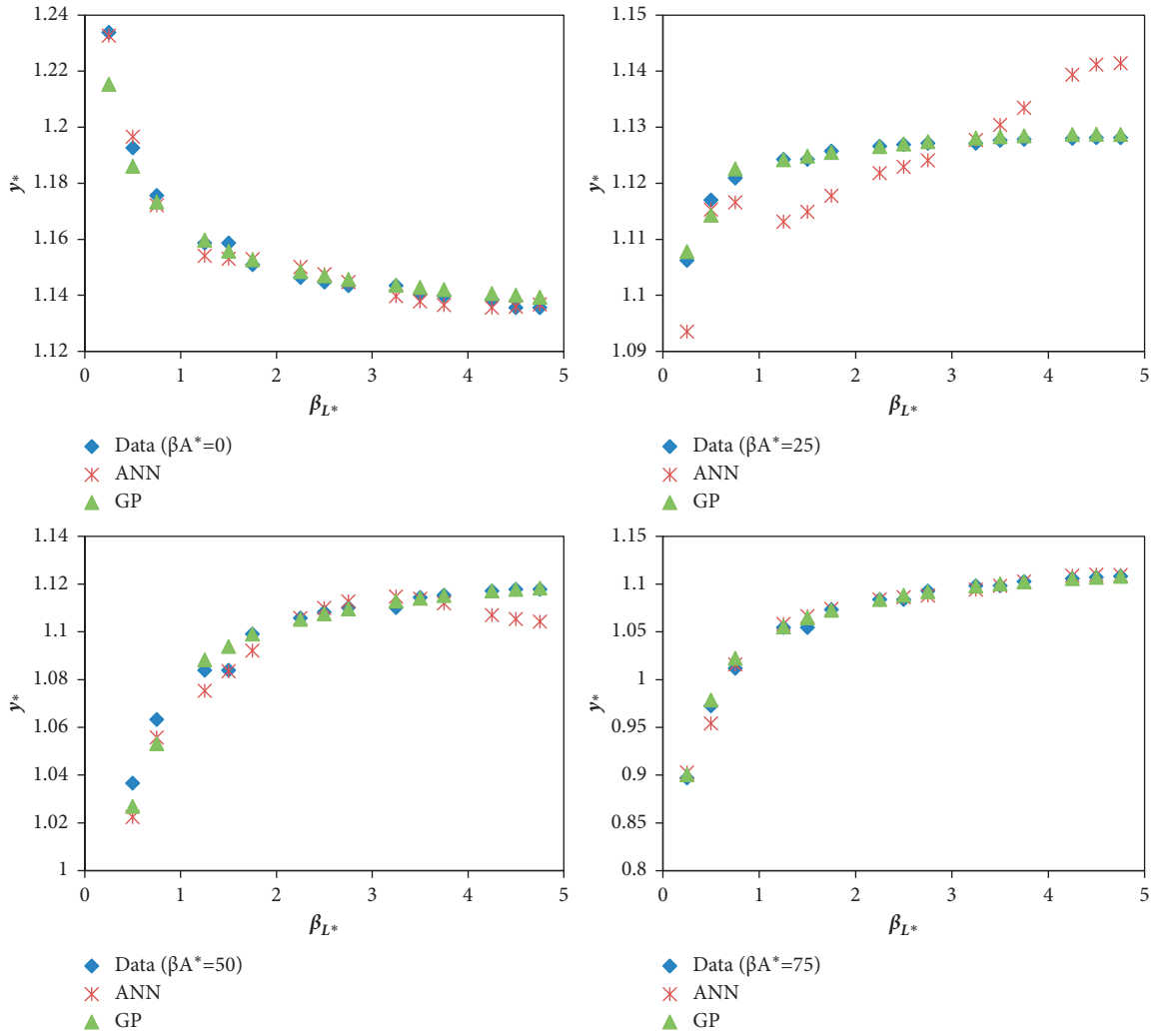

Figure 12: Comparison of the benchmark values of y^* with the estimations made by ANN and GP for the variable n scenario for the test data.

4. Conclusions

Conveying water from natural and artificial sources is substantially inevitable because of the distance between where water is in need and where water is available. In this study, the application of two ML models has been assessed for the optimum design of lined circular channels for the first time. The performances of these models were compared with those of explicit equations available in the literature for two scenarios: (1) flow-independent Manning's coefficient and (2) flow-dependent Manning's coefficient. Although the former may seem to be more suitable and streamlined to be used in practice, the latter has been approved by experimental studies. Since the variables involved in the design problem were normalized using a length-scale parameter, the solutions are not limited to a specific case study, whereas they embrace a variety combination of values for variables involved. According to the comparison, the ML models improved the prediction of geometries of circular channels estimated by the explicit equations between 55% and 88% based on RMSE, while the corresponding improvement range was between 62% and 91% based on MARE for both scenarios. Furthermore, the investigation of relative errors achieved by the ML models indicates that ANN and GP had quite similar performances. However, they had slightly different performances based on the scenario and channel geometry. To be more specific, for the constant roughness scenario, ANN performed slightly better than GP for calculating optimum values of dimensionless channel radius, while GP gave better results for optimum values of dimensionless water depth. On the other hand, GP results were a bit closer to the optimum solutions for calculating optimum values of circular geometries for the variable roughness scenario. Finally, the obtained results obviously demonstrate that not only applying AI models to the optimum design of circular channels yields closer results to the optimum solutions than using the available explicit equation but also considering a flow-dependent channel roughness in optimum design of lined circular channels may lead to solutions different from when a constant bed roughness is assumed.

Appendix

A. Comparison of the Benchmark Solutions with the ML Estimations

The benchmark solutions and outputs estimated by ANN and GP versus input variables are plotted for different scenarios. These plots are depicted in Figures 9–12. These figures provide the opportunity to investigate the effect of boundaries on the performance of the ML models. As shown, GP and ANN did perform acceptably in estimating the minimum and maximum values of output variables in most cases, while the former schematically performs even better than the latter in this regard. Since these figures do not provide qualitative information about the performances of the ML methods, they are presented here in Appendix A.

B. The ANN Output Equations

The output equation obtained by ANN is presented in the following equation [14]:

$$\text{output} = \text{linear}\{[\tanh(\text{input} \times IW + b_1)] \times LW + b_2\}, \tag{B.1}$$

where output is the channel property (r_* or y_*), $\text{linear}(x) = x$, $\tanh(x) = (2/1 + e^{-2x}) - 1$, input = $[\beta_{A*} \ \beta_{L*}]$ is the input matrix, and IW, LW, b_1, and b_2 are constant matrices (input weights, output weights, and biases). The constant matrices appeared in equation (B.1) depend on the roughness scenario (constant or variable n) and the channel property (r_* or y_*):

(a) Normalized radius (r_*) for constant roughness is as follows:

$$IW = \begin{bmatrix} -1.2747 & 4.7714 \\ 3.8194 & -1.9625 \\ -3.5514 & -1.5797 \\ 2.2211 & -3.1057 \\ -4.3712 & -1.3558 \\ -2.6416 & 1.9691 \\ 4.4975 & -0.7146 \\ 4.4073 & 2.2163 \\ -6.3307 & 1.4429 \\ 7.9585 & -1.7410 \end{bmatrix},$$

$$LW = [0.1089 \ \ 0.0313 \ \ 0.0138 \ \ -0.1659 \ \ 0.0145 \ \ 0.2045 \ \ 0.1898 \ \ 2.1255 \ \ 2.7497 \ \ 2.0036],$$

$$b_1 = \begin{bmatrix} 3.8295 \\ -3.0611 \\ 3.0218 \\ -0.1294 \\ 0.3099 \\ -1.5848 \\ 2.3836 \\ 7.7226 \\ -4.5416 \\ 5.6053 \end{bmatrix},$$

$$b_2 = [-2.1230]. \tag{B.2}$$

(b) Normalized water depth (y_*) for constant roughness is as follows:

$$IW = \begin{bmatrix} 1.8972 & -6.8594 \\ 4.5393 & -2.4272 \\ -4.1690 & -3.1827 \\ -3.0383 & -2.7364 \\ -1.3725 & 1.5407 \\ 8.3576 & -4.3048 \\ -4.4968 & 0.6641 \\ 10.8951 & -2.4065 \\ 6.4566 & -3.2644 \\ -4.0052 & -5.8913 \end{bmatrix},$$

$$LW = \begin{bmatrix} 0.0908 & -0.0453 & 0.2740 & -0.3087 & -0.3872 & -1.4087 & 0.1038 & 0.3004 & 1.7986 & 2.0548 \end{bmatrix},$$

$$b_1 = \begin{bmatrix} -5.9635 \\ -2.2562 \\ 2.6413 \\ 2.0764 \\ 0.1281 \\ 4.8110 \\ -1.4938 \\ 9.2226 \\ 3.7423 \\ -10.6689 \end{bmatrix}, \tag{B.3}$$

$$b_2 = [2.0829].$$

(c) Normalized radius (r_*) for variable roughness is as follows:

$$IW = \begin{bmatrix} 2.1051 & -3.4872 \\ 4.4230 & -0.4737 \\ -4.6699 & -1.4348 \\ 0.6999 & -2.8961 \\ -0.8608 & 1.9382 \\ 7.1420 & -1.1776 \\ -4.1166 & -1.1951 \\ 5.3566 & 1.3649 \\ 6.1985 & -1.1128 \\ -5.2261 & -1.5273 \end{bmatrix},$$

$$LW = \begin{bmatrix} -0.0366 & 0.0226 & 0.0043 & 0.2108 & 0.3665 & 2.6476 & -0.0298 & -2.0896 & -3.4226 & -2.1832 \end{bmatrix},$$

$$b_1 = \begin{bmatrix} -2.7516 \\ -2.6639 \\ 0.9685 \\ 1.6542 \\ -1.0562 \\ 6.2280 \\ -1.9247 \\ 5.5766 \\ 5.5902 \\ -5.6061 \end{bmatrix}, \tag{B.4}$$

$$b_2 = [0.1331].$$

(d) Normalized water depth (y_*) for variable roughness is as follows:

$$IW = \begin{bmatrix} 1.4323 & -5.3379 \\ 2.6917 & 2.9538 \\ -1.3738 & 5.4332 \\ 1.2035 & 0.4187 \\ 2.6227 & 3.3157 \\ -1.0381 & -3.5604 \\ -3.3328 & 0.2628 \\ 0.1158 & 4.9020 \\ 7.5539 & -1.3193 \\ 3.5985 & 1.9346 \end{bmatrix},$$

$$LW = \begin{bmatrix} -0.1947 & -0.1309 & 0.1458 & 0.3537 & -0.1333 & 0.3330 & -0.1289 & -0.1725 & 0.4865 & -1.6517 \end{bmatrix},$$

$$b_1 = \begin{bmatrix} -4.5318 \\ -3.8305 \\ 0.9470 \\ -0.7408 \\ -1.4023 \\ -2.7596 \\ -1.4157 \\ 0.6905 \\ 7.1377 \\ 6.2423 \end{bmatrix},$$

$$
\begin{aligned}
b_2 &= [1.4027],\\
C_* &= \frac{C}{\beta_E \lambda^2},\\
\beta_{A*} &= \frac{\beta_A \lambda}{\beta_E},\\
\beta_{L*} &= \frac{\beta_L}{\beta_E \lambda},\\
A_* &= \frac{A}{\lambda^2},\\
P_* &= \frac{P}{\lambda},\\
y_* &= \frac{y}{\lambda},\\
r_* &= \frac{r}{\lambda}.
\end{aligned}
\tag{B.5}
$$

Data Availability

The data used to support this study are obtained from the corresponding author upon request.

Conflicts of Interest

The author declares that there are no conflicts of interest.

References

[1] M. Niazkar, G. R. Rakhshandehroo, and S. H. Afzali, "Deriving explicit equations for optimum design of a circular channel incorporating a variable roughness," *Iranian Journal of Science and Technology, Transactions of Civil Engineering*, vol. 42, no. 2, pp. 133–142, 2018.

[2] S. M. Easa, "Open Channel cross section design: review of recent developments," in *Advances in Measurements and Instrumentation: Review (Chapter 6)*, S. Y. Yurish, Ed., vol. 1, International Frequency Sensor Association Publishing, Barcelona, Spain, 2018.

[3] B. Aksoy and A. B. Altan-Sakarya, "Optimal lined channel design," *Canadian Journal of Civil Engineering*, vol. 33, no. 5, pp. 535–545, 2006.

[4] Y.-C. Han and S. M. Easa, "Exact solution of optimum hydraulic power-law section with general exponent parameter," *Journal of Irrigation and Drainage Engineering*, vol. 144, no. 12, Article ID 04018035, 2018.

[5] B. R. Chahar and S. Basu, "Optimal design of curved bed trapezoidal canal sections," *Proceedings of the Institution of Civil Engineers-Water Management*, vol. 162, no. 3, pp. 233–240, 2009.

[6] S. M. Easa and A. R. Vatankhah, "New open channel with elliptic sides and horizontal bottom," *KSCE Journal of Civil Engineering*, vol. 18, no. 4, pp. 1197–1204, 2014.

[7] P. K. Swamee, "Optimal irrigation canal sections," *Journal of Irrigation and Drainage Engineering*, vol. 121, no. 6, pp. 467–469, 1995.

[8] P. K. Swamee, G. C. Mishra, and B. R. Chahar, "Minimum cost design of lined canal sections," *Water Resources Management*, vol. 14, no. 1, pp. 1–12, 2000.

[9] P. K. Swamee, G. C. Mishra, and B. R. Chahar, "Design of minimum earthwork cost canal sections," *Water Resources Management*, vol. 15, no. 1, pp. 17–30, 2001.

[10] P. K. Swamee and D. Kashyap, "Design of minimum seepage-loss nonpolygonal canal sections," *Journal of Irrigation and Drainage Engineering*, vol. 127, no. 2, pp. 113–117, 2001.

[11] P. K. Swamee and D. Kashyap, "Design of minimum seepage-loss nonpolygonal canal sections with drainage layer at shallow depth," *Journal of Irrigation and Drainage Engineering*, vol. 130, no. 2, pp. 166–170, 2004.

[12] M. Niazkar and S. H. Afzali, "Optimum design of lined channel sections," *Water Resources Management*, vol. 29, no. 6, pp. 1921–1932, 2015.

[13] P. K. Swamee and B. R. Chahar, *Design of Canals*, Springer, New Delhi, India, 2015.

[14] I. Ebtehaj, H. Bonakdari, and A. H. Zaji, "A new hybrid decision tree method based on two artificial neural networks for predicting sediment transport in clean pipes," *Alexandria Engineering Journal*, vol. 57, no. 3, pp. 1783–1795, 2018.

[15] M. Niazkar and M. Zakwan, "Assessment of artificial intelligence models for developing single-value and loop rating curves," *Complexity*, vol. 2021, Article ID 6627011, 21 pages, 2021.

[16] M. Zakwan and M. Niazkar, "A comparative analysis of data-driven empirical and artificial intelligence models for estimating infiltration rates," *Complexity*, vol. 2021, Article ID 9945218, 13 pages, 2021.

[17] M. Niazkar, F. Hajizadeh mishi, and G. Eryılmaz Türkkan, "Assessment of artificial intelligence models for estimating lengths of gradually varied flow profiles," *Complexity*, vol. 2021, Article ID 5547889, 11 pages, 2021.

[18] M. Niazkar, "Assessment of artificial intelligence models for calculating optimum properties of lined channels," *Journal of Hydroinformatics*, vol. 22, no. 5, pp. 1410–1423, 2020.

[19] A. M. Tawfik, "Design of channel section for minimum water loss using Lagrange optimization and artificial neural networks," *Ain Shams Engineering Journal*, vol. 12, no. 1, pp. 415–422, 2021.

[20] M. Niazkar, N. Talebbeydokhti, and S. H. Afzali, "One dimensional hydraulic flow routing incorporating a variable grain roughness coefficient," *Water Resources Management*, vol. 33, no. 13, pp. 4599–4620, 2019.

[21] S. K. McKay and J. C. Fischenich, *Robust Prediction of Hydraulic Roughness, ERDC/CHL CHETN-VII-11*, U.S. Army Engineer Research and Development Center, Vicksburg, MS, USA, 2011.

[22] D. L. Yarnell and S. M. Woodward, *The Flow of Water in Drain Tile*, US Department of Agriculture, Washington, DC, USA, 1920.

[23] E. R. Wilcox, "A comparative test of the flow of water in 8-inch concrete and vitrified clay sewer pipe," *Engineering Experiment Station. Engineering Experiment Station Series. Bulletin*, Seattle, Wash., The University Washington (State) University, Seattle, WA, USA, 1924.

[24] N. A. Zaghloul, "Gradually varied flow in circular channels with variable roughness," *Advances in Engineering Software*, vol. 15, no. 1, pp. 33–42, 1992.

[25] Ö. Akgiray, "Simple formulae for velocity, depth of flow, and slope calculations in partially filled circular pipes," *Environmental Engineering Science*, vol. 21, no. 3, pp. 371–385, 2004.

[26] M. Niazkar and S. H. Afzali, "Developing a new accuracy-improved model for estimating scour depth around piers using a hybrid method," *Iranian Journal of Science and Technology, Transactions of Civil Engineering*, vol. 43, no. 2, pp. 179–189, 2018.

[27] F. D. Francone, *Discipulus Owner's Manual*, Machine Learning Technologies, Inc, Littleton, CO, USA, 1998.